Toxicology in Vitro 48 (2018) 276–285

Contents lists available at ScienceDirect

Toxicology in Vitro

journal homepage: www.elsevier.com/locate/toxinvit

Biocompatibility of pristine graphene monolayer: Scaffold for fibroblasts

Iwona Lasocka[a], Lidia Szulc-Dąbrowska[b], Michał Skibniewski[c,*], Ewa Skibniewska[a], Włodzimierz Strupinski[d,e], Iwona Pasternak[d,e], Hubert Kmieć[a], Paweł Kowalczyk[f]

[a] Department of Biology of Animal Environment, Faculty of Animal Science, Warsaw University of Life Sciences, Ciszewskiego street 8, 02-786 Warsaw, Poland
[b] Department of Preclinical Sciences, Faculty of Veterinary Medicine, Warsaw University of Life Sciences, Ciszewskiego street 8, 02-786 Warsaw, Poland
[c] Department of Morphological Sciences, Faculty of Veterinary Medicine, Warsaw University of Life Sciences, Nowoursynowska street 159, 02-776 Warsaw, Poland
[d] Institute of Electronic Materials Technology, Wólczyńska street 133, 01-919 Warsaw, Poland
[e] Faculty of Physics, Warsaw University of Technology, Koszykowa street 75, 00-662 Warsaw, Poland
[f] Department of Animal Nutrition, The Kielanowski Institute of Animal Physiology and Nutrition, Polish Academy of Sciences, Instytucka street 3, 05-110 Jabłonna, Poland

ARTICLE INFO

Keywords:
Graphene
Cytotoxicity
Cytoskeleton
Migration
Focal adhesion

ABSTRACT

The aim of the present study was to evaluate the cytotoxicity of pristine graphene monolayer and its utility as a scaffold for murine fibroblast L929 cell line. Cell viability, morphology, cytoskeleton architecture (microfilaments and microtubules), cell adhesion and migration into the scratch-wound area were determined using pristine graphene-coated microscopic slides. We found that fibroblasts cultured on pristine graphene monolayer exhibited changes in cell attachment, motility and cytoskeleton organization. Graphene was found to have no cytotoxicity on L929 fibroblasts and increased cell adhesion and proliferation within 24 h of culture. The area of cells growing on graphene was comparable to the area of fibroblasts cultured on glass. Migration of cells on the surface of graphene substrate appeared to be more regular in comparison to uncoated glass surface, however in both control (glass) and experimental (graphene) groups the scratch wound was closed after 48 h of culture. Taken together, our results indicate that pristine graphene monolayer is non-toxic for murine subcutaneous connective tissue fibroblasts and could be beneficial for recovery of damaged tissues after injury. These studies could be helpful in evaluating biocompatibility of graphene, which still remains ambiguous.

1. Introduction

Methods of tissue engineering allow for the development of new therapeutic strategies for tissue injury. There has been tremendous progress in the methodical development of large-scale *in vitro* cell culture and the synthesis of cellular scaffolding materials. Scaffolds used in cellular engineering not only have supporting functions, but also stimulate tissue regeneration at the site of injury. Choosing a suitable material for tissue engineering is crucial for medical applications and achieving therapeutic results. Such material must not be cytotoxic or mutagenic, and must also have adequate physicochemical properties that will ultimately provide a favorable environment for adhesion, proliferation and cell differentiation (Bacakova et al., 2011). So far many materials have been tested. In recent years one such material, graphene, isolated and characterized in 2004, has attracted attention as a promising material in tissue regeneration.

Graphene is a single-atom-thick sheet of sp2-bonded carbon atoms. It is a unique form of carbon in which the atoms are arranged in a hexagon. Graphene has unique physical, chemical, electrical and mechanical properties, which qualify it as a promising nanomaterial in areas such as physics, material science and other technological applications (Park et al., 2009). Some investigations indicate that graphene could have great potential for bacterial inhibition, drug delivery and photo-thermal therapy (Goenka et al., 2014; Akhan and Ghaderi, 2010). Cytotoxicity tests have been widely performed to assess the cytotoxic effect on different biomaterials and to determine biocompatibility. The International Standards Organization (ISO10993-5) classifies the cytotoxicity assay as the first step in the sequence of biocompatibility tests (Poskus et al., 2009). The direct contact method with L929 cells is one of the most frequently used for evaluating the cytotoxicity and may represent a sufficient screening model for *in vitro* evaluation of cytotoxicity (Park et al., 2002). Cytocompatibility of biomaterial can be assessed based on the cell cytoskeleton organization. The cellular cytoskeleton is a flexible and dynamic protein filament system composed of microfilaments, intermediate filaments and microtubules, which together with their associated proteins form a network that connects the cell nucleus, organelles and cytoplasmic membrane. The cytoskeleton determines the shape and movement of organelles throughout the

* Corresponding author.
E-mail address: michal_skibniewski@sggw.pl (M. Skibniewski).

https://doi.org/10.1016/j.tiv.2018.01.028
Received 19 September 2017; Received in revised form 29 December 2017; Accepted 30 January 2018
Available online 01 February 2018

whole cell and plays an important role in cell division, transport, apoptosis and proliferation (Mogilner and Keren, 2009; Tschumperlin, 2013; Atherton et al., 2015). It's primary role is to contribute to the spatial organization of the cytoplasm, where it creates a specific scaffold for proteins involved in various intracellular processes. The dynamic reorganization of the actomyosin cytoskeleton in response to various stimuli is at the base of all phenomena related to cellular motility (Lange and Fabry, 2013). Cells creep upon the surface, have morphologically and functionally differentiated front and back region (motion polarization) (Tojkander et al., 2012). This phenomenon is well visible during cell migration in the scratch wound assay. The force required for cell movement is generated by processes occurring in the cortical cytoskeleton, which is located under the cell membrane. The organization of cortical cytoskeleton depends on actin-binding regulatory proteins (Furuhashi et al., 2012). Bunches of contractile actin filaments run parallel to the cell membrane and are attached to the adhesive “bands” by a complex of intracellular linking proteins, such as vinculin (Furuhashi et al., 2012). Vinculin is a protein associated with the cytoplasmic surface of adhesive plaques, which anchors microfilaments containing actin in the cell membrane and attach the cell to the ground (Peng et al., 2011; DeMali et al., 2014; Atherton et al., 2015). The role of vinculin in cell adhesion sites has been described by Atherton et al. (2015). Flat, elongated structures rich in heterodimeric (α and β) cell adhesion receptors produce focal contacts - dynamic macromolecular complexes containing integrins. Cytoplasmatic tails of integrins bind to a wide spectrum of proteins that regulate activation and their interaction with the extracellular matrix. These focal adhesion proteins also send and respond to the extracellular signals and physical properties of the extracellular matrix and provide a physical linkage between the integrins and the cytoskeletal network of actin. Vinculin is recruited into the cytoplasmic tails of β-integrin proteins by interacting with the talin (Burridge and Mangeat, 1984; Yao et al., 2014). A study by Saunders et al. (2006) demonstrated that the presence of vinculin in the focal contacts is crucial for cell adhesion and migration *via* the integrin-actin linkage system. Vinculin reduces cellular motility by affecting cell adhesion: cells lacking vinculin evince less adhesion but faster migration. Conversely, in cells overexpressing vinculin, the number and size of focal contacts increase, whereas motility decreases. Visualization of vinculin is one of the methods of cell adhesion evaluation to various types of substrates (Furuhashi et al., 2012; Tan et al., 2015; Wytrwal et al., 2016). Another part of the cytoskeleton are microtubules. They are made up of polymerised α- and β-tubulin dimers, which build protofilaments and have a distinct polarity. Microtubules play a crucial role during cell migration; they are able to grow and shrink in order to generate force to remodel. Microtubules also control focal adhesion dynamic in migrating cells by modulating Rho GTPase signaling that control actomyosin-based contractility (Stehbens and Wittmann, 2012).

The graphene substrates affect the adhesion and proliferation of various adherent cells (Kalbacova et al., 2010; Tan et al., 2015) and may be used in tissue engineering (Lee et al., 2013; Gurunathan et al., 2014). The effect of graphene on the cytoskeleton of migrating fibroblasts, with particular emphasis on vinculin, has never been studied before. Therefore, in the present study we evaluated the rearrangement and architecture of cellular cytoskeleton (microfilaments and microtubules) and vinculin organization in L929 fibroblasts in response to this substrate produced by the Institute of Electronic Materials Technology (ITME) (Strupinski, 2011; Strupinski et al., 2011; Ciuk et al., 2013). We focused on the basic methods used in material toxicity assessment and the organization of the cellular cytoskeleton with particular emphasis on changes in adhesion and migration of fibroblasts on two different substrates, glass and graphene. Data on structural characteristics of cells will help to understand how fibroblasts move on the graphene substrate and whether graphene is safe for cytoskeletal components. These tests can be used to evaluate the usefulness of graphene as a scaffold for connective tissue cells that could be used as potential “dressings” in the treatment of tissue injury in the future.

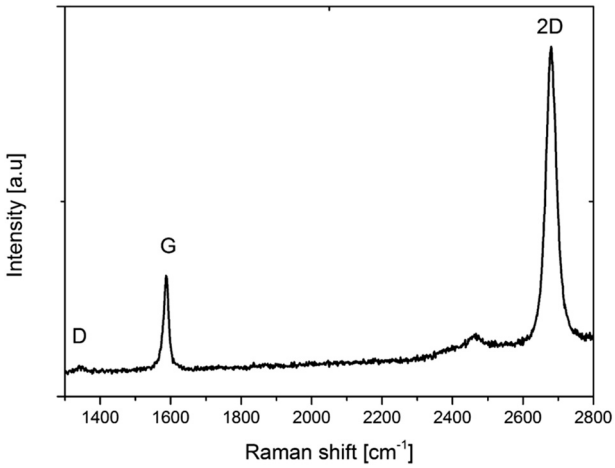

Fig. 1. Raman spectrum of graphene.

2. Materials and methods

2.1. Material

Production of graphene was conducted by chemical vapor deposition (CVD) of volatile phases in a CVD reactor Black Magic Pro 6″. Studies described in this report were carried out with graphene produced on copper substrate, and then transferred onto rounded glass cover slips (1 cm diameter and 0.17 mm of thickness) at the Institute of Electronic Materials Technology (ITME). Electrochemical delamination was used in the transfer process (Ciuk et al., 2013). A sheet of graphene was placed on a cover slide. Cover slides coated with graphene were sterilized by UV (30 min. on the both sides) and placed into wells of a 24-well plate. The quality of each preparation was certified, by measuring Raman spectrum with characteristic peaks marked (Fig. 1), and optical microscope picture of graphene on a cover glass (Fig. 2). Raman spectrum of graphene proves existing of monolayer graphene on glass substrate (Ferrari et al., 2006; Gupta et al., 2006; Graf et al., 2007; Lee et al., 2008). Low Full Width at Half Maximum (FWHM about 34,6 cm^{-1}) of the 2D band for graphene layer presented in Fig. 1 as well as much higher (I_{2D}/I_G = 2,9) intensity of the 2D band by comparison with the intensity of the G band are characteristic of a single layer of graphene. Very low D bands on spectrum is typical of high quality graphene structures (A_D/A_G = 0,09). Additionally, optical microscope image confirmed that graphene is uniform when it comes to its

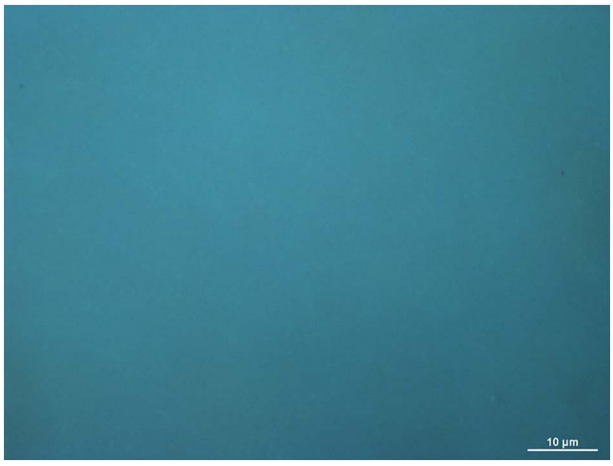

Fig. 2. Optical microscope image of graphene applied on glass cover slide.

thickness and continuous (no holes or tears).

2.2. Cell culture

L929 cell line (CCL-1) derived from normal subcutaneous areolar and adipose tissue of C3H/An mouse was obtained from the American Type Culture Collection (ATCC). Cells were cultured in high glucose DMEM (Dulbecco's Modified Eagle's Medium, HyClone, USA) supplemented with 5% fetal bovine serum (FBS; Sigma-Aldrich) and 1% antibiotic-antimycotic solution containing 100 U/ml penicillin, 100 µg/ml streptomycin, and 0.25 µg/ml amphotericin B (Sigma-Aldrich). Cells were incubated at 37 °C in a 5% CO_2 humidified atmosphere.

Unless otherwise specified, in all experiments, L929 cells (5×10^4/well) were seeded onto sterile microscopic glass coverslips (control) and graphene-coated glass coverslips placed in 24-well plates (Falcon, USA). After 1, 3, 12 and/or 24 h cells were harvested for further experiments.

2.3. Cell morphology evaluation

Morphology of L929 fibroblasts was observed at 1, 3, 12 and 24 h of cell seeding on control or graphene-coated microscopic slides. Images were captured with an inverted microscope (Olympus IX71) equipped with Color View III cooled CCD camera and CellˆF software (Soft Imaging System) (Olympus, Japan).

2.4. Cell viability

L929 cells grown for 24 h on glass coverslips (control) or graphene-coated microscopic slides (experimental) were detached with trypsin-EDTA (Ethylenediamine tetra-acetic acid) solution (HyClone, USA). Collected cells were centrifuged and the cell pellet was washed with serum-free culture medium. Next, the cell suspension was mixed 1:1 with a 0.4% Trypan Blue solution (Sigma-Aldrich) and the mixture was transferred to a Neubauer chamber. Trypan Blue exclusion was used to calculate the relative proportion of the dead cells. The results were expressed as a percentage of viable cells.

2.5. Cell proliferation (mitochondrial activity-based assay)

Cell Counting Kit-8 (CCK-8, Sigma-Aldrich) is a colorimetric assay for determination of viable cell numbers, measuring mitochondrial activity as well as cytotoxicity. CCK-8 uses a tetrazolium salt, WST-8 (2-(2-methoxy-4-nitrophenyl)-3-(4-nitrophenyl)-5-(2,4-disulfophenyl)-2H–tetrazolium, monosodium salt), which produces water soluble WST-8 formazan. CCK-8 solution is very stable and has negligible cytotoxicity. The detection sensitivity is higher than any other tetrazolium salts such as MTT, XTT or MTS. The amount of formazan produced is directly proportional to the number of living cells.

2.5.1. Standard curve derivation

Two-fold serial dilutions of L929 cells were made in 96-well microliter plates, in triplicates. Next, 10 µl of CCK-8 reagent was added to each well of the standard curve and incubate for 2 h at 37 °C in a humidified atmosphere of 5% CO2 in air. The absorbance of triplicate serial dilutions in 96-well plate was determined at 450 nm using Epoch Microplate Spectrophotometer (BioTek, Winooski, VT, USA). Negative control containing media only (no cells) was used for background measurement. The range of the standard curve sensitivity for L929 was approximately 3 × 104–2.34 × 102 cells/ml.

2.5.2. Control and experimental samples

The standard curve was run concurrently with all test samples. L929 cells grown for 24 h on glass coverslips only (control) or graphene-coated glass coverslips (experimental) were detached with trypsin-EDTA solution and resuspended in appropriate culture medium. Cells in a total volume of 100 µl were added in triplicate to a 96-well plate. 10 µl of WST-8 reagent was added to each well (three controls and three experimental) and the plates were incubated at 37 °C in a humidified CO_2 incubator for 2 h. Absorbance was determined at 450 nm using a spectrophotometer. The mitochondrial activity of cells growing on graphene-coated slides was calculated from the standard curve in relation to the control group (without graphene).

2.6. Cytotoxicity - direct contact method

Cytotoxicity of graphene in the direct contact method with L-929 mouse fibroblast was conducted using the criteria described earlier by Jesion et al. (2015). Briefly, the degree of toxicity of graphene was evaluated basing on cell morphology, viability (trypan blue test) and mitochondrial activity (WST-8 test). All assays were done in triplicate.

2.7. Wound healing assay

L929 cell motility was assessed using the wound-healing assay. Fibroblasts were plated on graphene-coated coverslips or not in 24-well plates and cultured for 24–48 h to achieve a sub-confluent cell monolayer. A scratch was made on the cell layer using a sterile micropipette tip. Floating cells were removed by gently washing with culture medium (with 1% FBS) three-times. Cells were then incubated for 0, 18, 24 and 48 h at 37 °C in a humidified atmosphere of 5% CO_2 in the air. Phase-contrast photographs were taken at the same area of the wound using Color View III cooled CCD camera (Olympus) mounted on an inverted microscope Olympus IX71. Artificial lines fitting the cutting edges were drawn on pictures of the selected original wounds. Cell migration was assessed by counting the number of cells that had migrated into the wound area (Szulc-Dabrowska et al., 2016). Three independent experiments were performed in duplicate. Single cell-area was measured using ImageJ software.

2.8. Immunofluorescence staining

For F-actin or vinculin detection, cells were fixed in 4% paraformaldehyde (PFA, Sigma-Aldrich) in PBS for 20 min. For α-tubulin detection, cells were fixed in ice-cold 100% methanol for 2 min. Fixed cells were permeabilized with 0.5% Triton X-100 (Sigma-Aldrich) in PHEM buffer (Pipes-Hepes-EGTA-$MgCl_2$) prepared as previously described (Schliwa and Blerkom, 1981) and blocked with 3% bovine serum albumin (BSA, Sigma-Aldrich) in PHEM-Triton X-100 (0.1%). Next, slides were incubated with fluorescein isothiocyanate (FITC)-conjugated phalloidin (Sigma-Aldrich) for 20 min. or with primary antibodies (Abs) directed against α-tubulin or vinculin (both from Sigma-Aldrich) for 30 min. To detect primary Abs, cells were incubated with appropriate secondary Abs: donkey anti-mouse IgG or goat anti-rabbit IgG conjugated with FITC or rhodamine Red-X for 30 min. DNA was stained with 1 µg/ml Hoechst 33,342 (Sigma-Aldrich) for 2.5 min. Slides were mounted in ProLong Gold Antifade Reagent (Invitrogen, USA) and examined using a fluorescence microscope Olympus BX60 equipped with Color View III cooled CCD camera. Images were analyzed using CellˆF and ImageJ software.

2.9. Statistical analysis

Three independent experiments were performed. Results were expressed as mean ± standard deviation (SD). Statistical analysis was carried out using Statistica 12.0™ (StatSoft Poland) software and based upon the one-way analysis of variance (ANOVA) with post-hoc Tukey's tests. The differences were considered significant from $p \leq 0.05$.

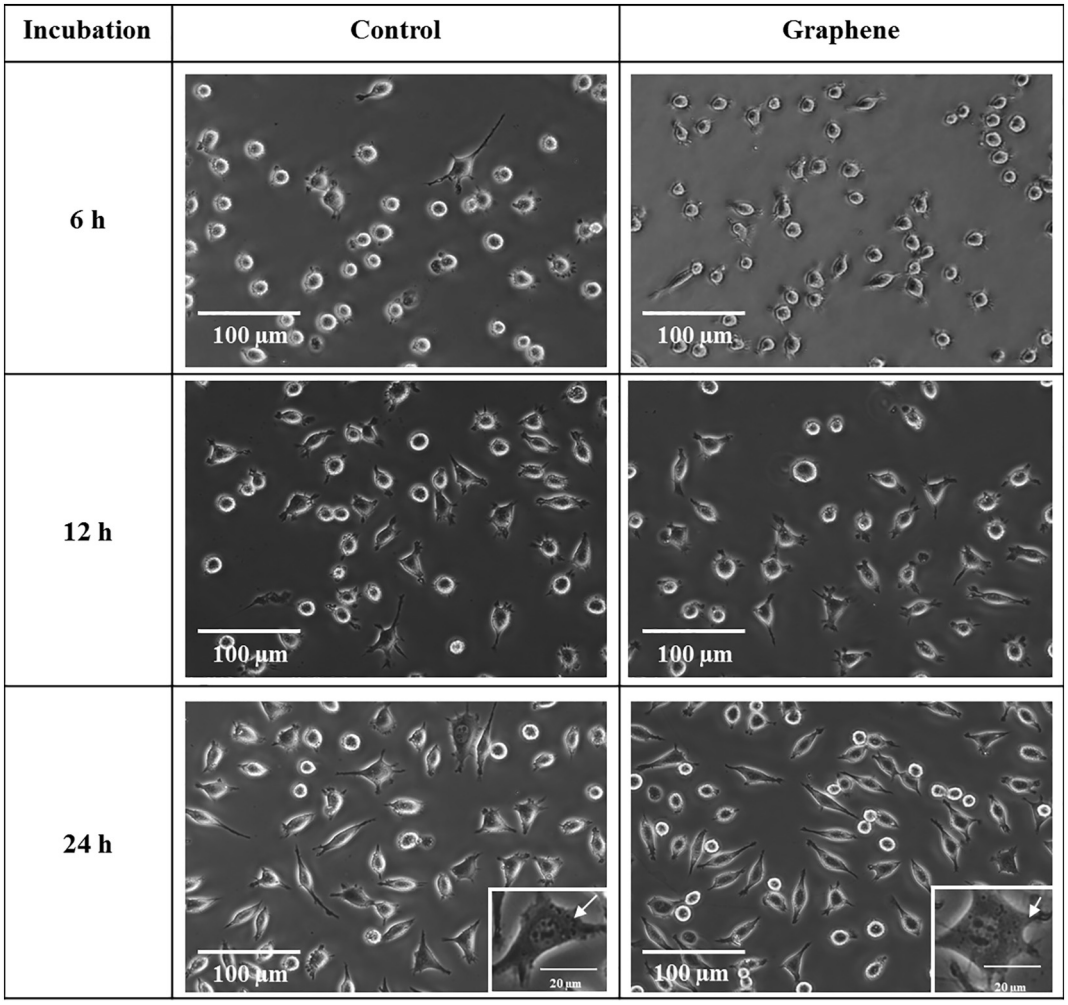

Fig. 3. Morphology of L929 fibroblasts grown on glass (control) or graphene. Phase-contrast images of cells incubated with or without graphene for 6, 12 and 24 h.

3. Results

3.1. Cell morphology, viability and proliferation on pristine graphene monolayer

On both control and graphene-coated slides, morphological changes were detected after six hours of incubation. Round shaped cells gradually changed into a spindle form. Morphological changes were pronounced at 12 h of incubation, with the tendency of lamellipodia and filopodia formation. At 24 h of incubation, most of the cells were characterized by modified morphology in relation to the forms observed immediately after seeding on both control and graphene-coated surfaces (Fig. 3). In both groups, spindle cells with single, clearly visible nuclei with one or more nucleoli were observed. The cells on both surfaces were similarly characterized by cytoplasmic granules.

Trypan blue exclusion is a widely used assay in cytotoxicity testing for staining of dead and live cells. Generally, cell viability between 95 and 99% is regarded as good. In the present study the viability of L929 cells cultured on graphene was 96 ± 2% and statistical analysis revealed no significant differences ($p \leq 0.05$) compared to viability of control cells (95 ± 1.5%). Further, a proliferation assay based on mitochondrial activity was performed using CCK-8 as described by Liao et al. (2011). The proliferation of cells grown on graphene was significantly ($p < 0.01$) higher (113.5 ± 3.2%) in comparison to the control group (100 ± 3.8) (Fig. 4).

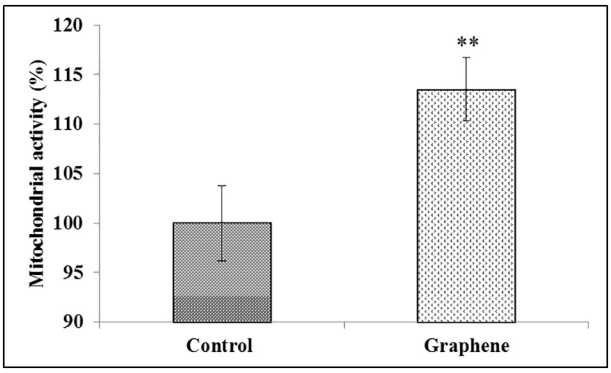

Fig. 4. Mitochondrial activity (proliferation assay) of L929 fibroblasts grown on glass or graphene substrate. Data are represented as mean ± SD (standard deviation) of three independent experiments. $^{**}p < 0.01$.

3.2. Pristine graphene monolayer is not cytotoxic for L929 fibroblasts

L929 cells cultured on graphene did not show lytic reaction as observed under microscopy (Fig. 3). Similar to control cells, fibroblasts grown on graphene showed no reduction of cell growth (Fig. 4), the presence of single cytoplasmic granules (Fig. 3), and < 5% of cells became rounded, shrunk or detached from the slides. Based on our observations, we conclude that graphene has no cytotoxic activity on L929 fibroblasts, determined according to PN-EN ISO 10993-5 as grade

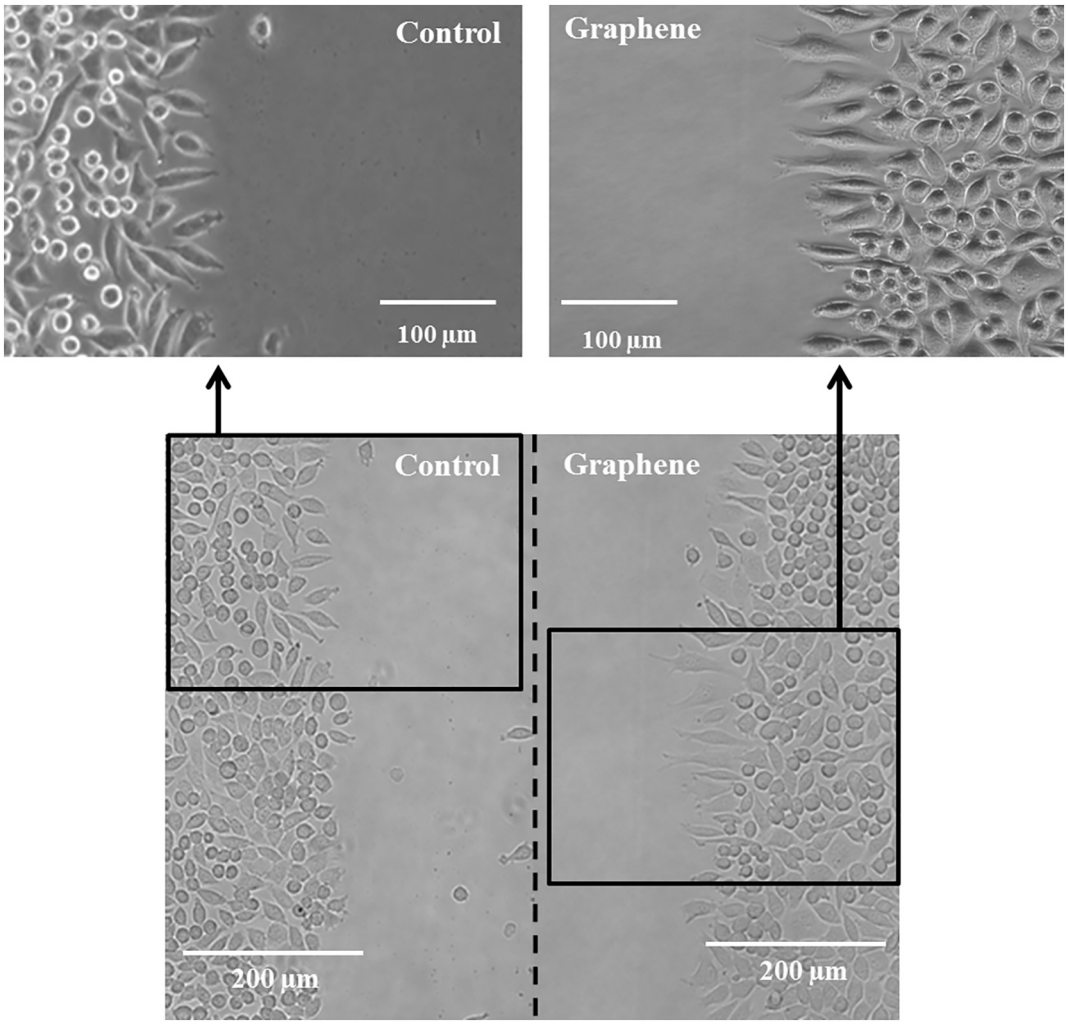

Fig. 5. Polarization of L929 cells grown on glass and graphene substrate. Scratch wound healing assay of L929 cells plated on glass or pristine graphene monolayer. Representative phase-contrast images of cells at 3 h after scratch. The magnified images are of the boxed region.

0 (ISO, 2009).

3.3. L929 fibroblasts cultured on pristine graphene monolayer migrate more evenly into the wound

The wound-healing assay was used to evaluate L929 cell migration on glass or graphene-coated slides. After 3 h of wound induction, glass- and graphene-cultured cells were found at the wound edge. Cells exhibited elongated and polarized morphology consisting of a leading edge lamellipodia and a trailing tail (Fig. 5). Closure of the "wound" in the experimental group occurred as a result of organized fibroblast migration from both edges of the scratch (Fig. 6). Cell migration in the control group was less organized. The complete closure of the wound occurred after 48 h, in both, control and experimental groups. Statistical analysis revealed that the mean area of fibroblasts migrating into the scratch was comparable ($p > 0.05$) between both groups, however cells on the graphene substrate had slightly larger area (by 60 μm^2) than control cells (Fig. 7).

3.4. Pristine graphene monolayer does not induce reorganization of actin microfilaments and microtubules, however increases focal adhesion formation in L929 fibroblasts

Our last question concerned the effect of pristine graphene monolayer on cytoskeleton organization in L929 fibroblasts. We performed fluorescence microscopy analysis of structures formed by different cytoskeletal proteins: F-actin (filamentous actin bundles and stress fibers within the cytoplasm, lamellipodia and filopodia on the leading edge of the moving cell], α-tubulin [microtubule-organizing center (MTOC), cytoplasmic microtubules] and vinculin (focal adhesion). F-actin staining revealed that L929 cells did not show morphology abnormalities during cultivation on graphene substrate. Within the cells of both groups actin filaments were highly concentrated at the cell periphery and formed a cell cortex (Fig. 8). Additionally, stress fibers consisted of large bundles of actin filaments were clearly visible. The stress fibers and the focal adhesions (vinculin-based staining) were located along the cell, however these structures were more evident in cells growing on graphene (Figs. 8, 9). Statistical analysis revealed that cells grown on graphene produced more focal adhesions primarily in the peripheral areas of the cell (Fig. 10). Moreover, in graphene-cultured cells predominant actin filament structures were stress fibers (Figs. 8 and 9). F-actin is linked by the vinculin tail, and the head of vinculin joins with the talin, which connects to integrins that penetrate the cell membrane and bind to extracellular matrix (ECM) (Furuhashi et al., 2012; Atherton et al., 2015; Yao et al., 2014). The connections between F-actin with vinculin are clearly visible on Fig. 8. Such connections regulate actin dynamics and recruit actin filaments to the growing focal adhesions (Atherton et al., 2015; Yao et al., 2014). Taken together, our results indicate that graphene increases contact adhesion of L929 cells.

Cell movement would not be possible without the presence of

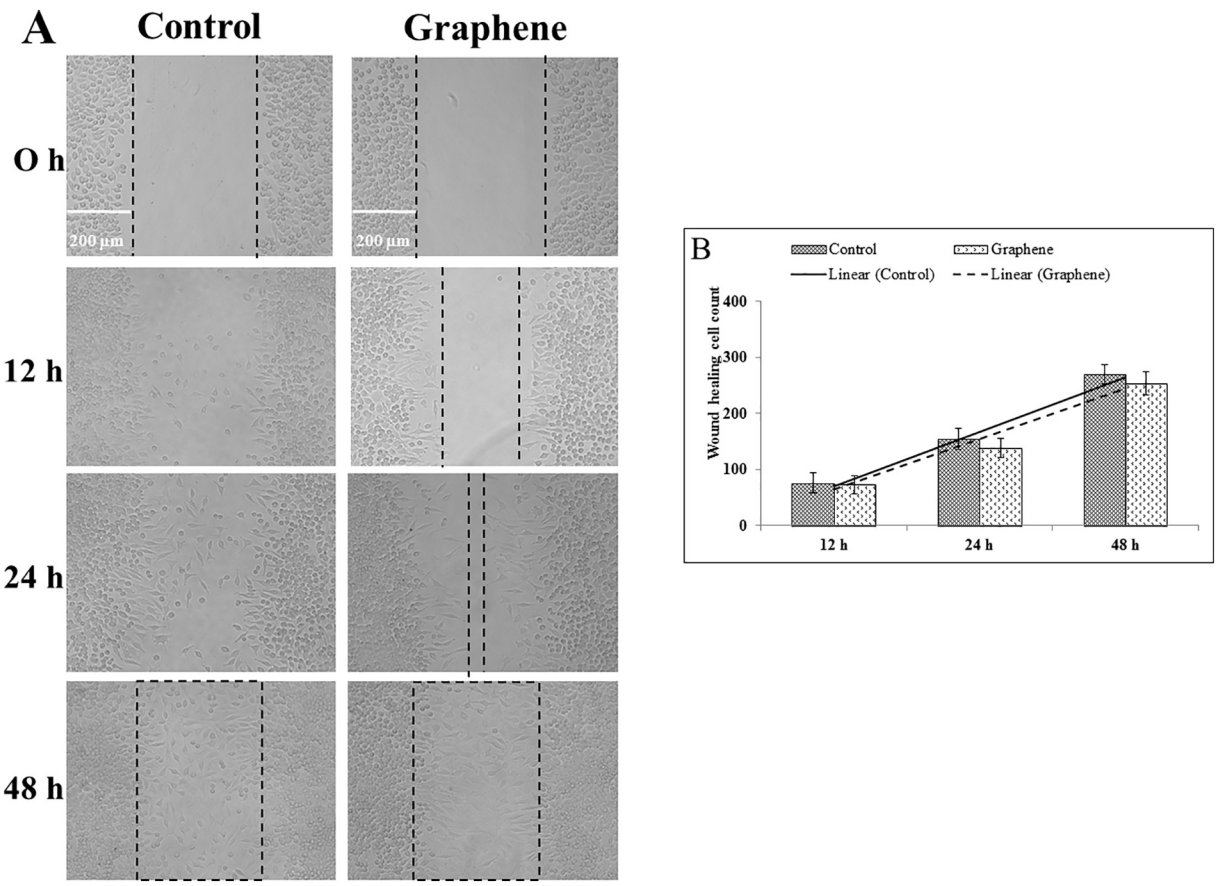

Fig. 6. Migration of L929 cells on graphene. (A) Scratch wound healing assay of L929 cells plated on glass and graphene. Representative phase-contrast images of cells at time 0, 12, 24 and 48 h. (B) The number of cells migrated into the scratch area. Data are represented as mean ± SD (standard deviation) of three independent experiments.

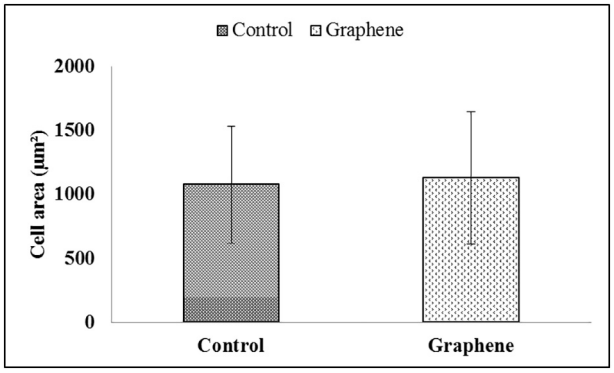

Fig. 7. Effect of graphene on L929 cell area. Data are represented as mean ± SD (standard deviation) of three independent experiments.

microtubules, which together with motor proteins (dyneins, kinesins) transport organelles and vesicles. Fluorescence staining of α-tubulin showed that the organization of microtubule network in glass- and graphene-cultured cells was similar (Fig. 11). The microtubules were composed of thick and intertwined filaments, which radiated from the microtubule organizing center (MTOC) and branched toward the edge of the cell, creating a system of trails. Thus, graphene does not alter the microtubule network organization in L929 fibroblasts.

4. Discussion

Cytotoxicity tests are necessary for preliminary assessment of safety of materials used in regenerative medicine. Many valuable properties of graphene (antibacterial, antiviral, anticancer) have been shown in numerous studies (Akhan and Ghaderi, 2010; Wang et al., 2011, 2012, 2016; Goenka et al., 2014; Sawosz et al., 2015; Zhang et al., 2016). Some authors suggest that graphene and its derivatives are strong candidates as tissue scaffold or functional coating material for biomedical applications (Kalbacova et al., 2010; Chen et al., 2012; Lee et al., 2013; Gurunathan et al., 2014; Jesion et al., 2015; Tan et al., 2015; Verdanova et al., 2016; Wang et al., 2016;), whereas others pay attention to its potential toxicity for various cell types (Liao et al., 2011; Wojtoniszak et al., 2012; Guo and Mei, 2014; Zhang et al., 2016; Zhou et al., 2017). These contradictory reports may be a result of different physical and chemical properties of the studied 'graphene-family nanomaterials', what could be caused for example by: different layers, dimensions, concentration, hydrophilicity, stiffness, surface modifications and purity of the tested material. In the present study we evaluated cytotoxicity of single-layer pristine graphene for L929 fibroblasts. L929 cells are commonly used in cytotoxicity tests. Our interest in these cells also stems from the fact that fibroblasts play a key role in the wound healing process. We supposed that graphene, due to its properties, could be a potential candidate as fibroblast scaffold when applied on the wound to accelerate the healing process. Assessment of graphene cytotoxicity on L929 is the first step in this direction.

Wang et al. (2016) have shown that the addition of pristine graphene to ε-caprolactone as a 3-D scaffold had a positive impact on cell viability and proliferation of human adipose-derived stem cells. They also have noticed that the cell proliferation rate increased in a dose-dependent manner of graphene administration. Our results indicate that graphene promotes proliferation of L929 cells, since mitochondrial activity was about 12% higher than that observed in control fibroblasts cultured on non-graphene-coated surface. Graphene is naturally hydrophobic, however the topography of the scaffold and its roughness may affect surface wettability and, in consequence, affect the

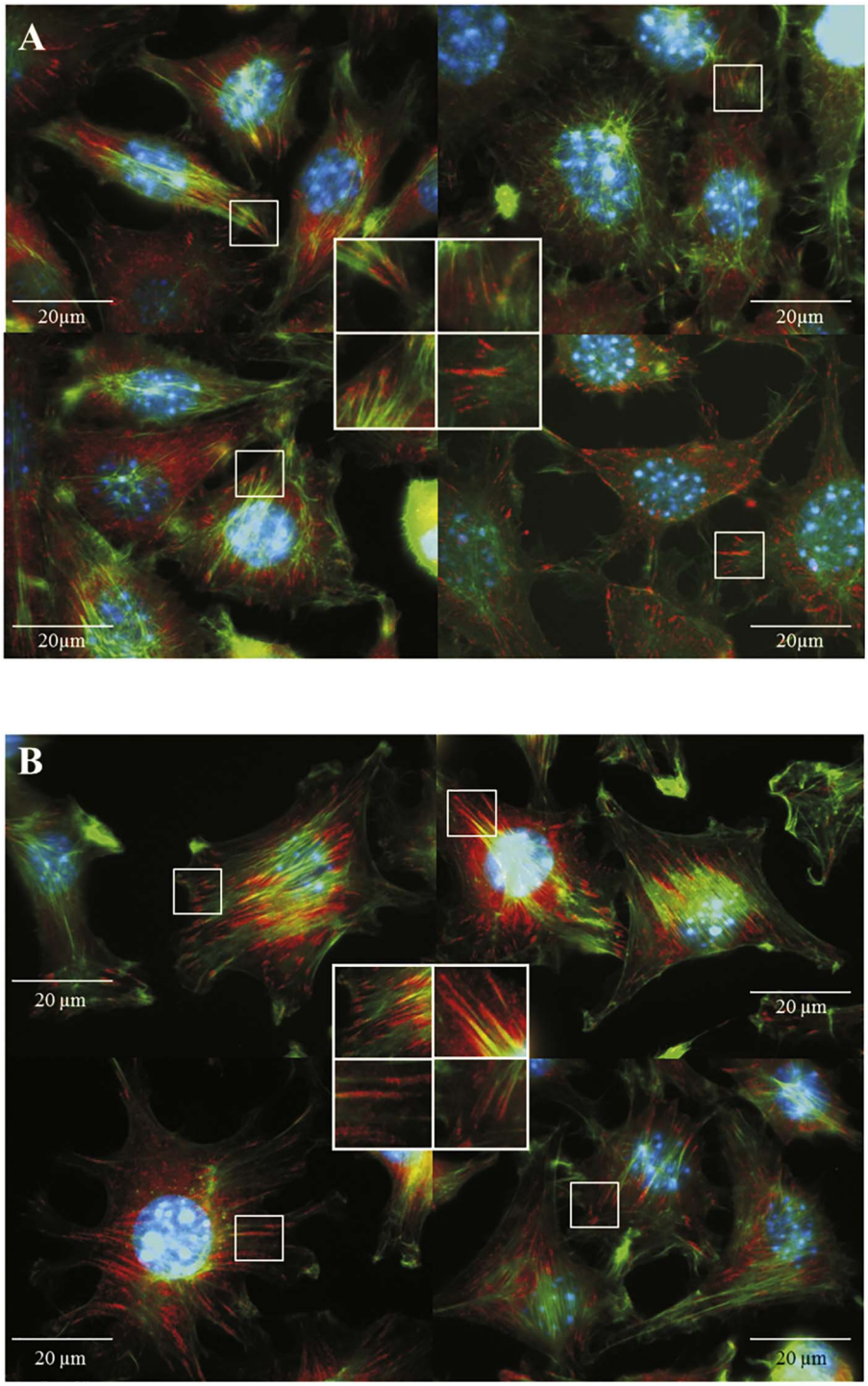

Fig. 8. The interactions between vinculin and F-actin in L929 cells. Cells were incubated for 24 h on glass (A) and pristine graphene monolayer (B) and stained with phalloidin-FITC (F-actin, green fluorescence), anti-vinculin Abs (vinculin, red fluorescence) and Hoechst 33,342 (DNA, blue fluorescence). The magnified images are of the boxed regions. (For interpretation of the references to color in this figure legend, the reader is referred to the web version of this article.)

proliferation of cells (Kalbacova et al., 2010). In subsequent studies Kalbacova et al. (2014) have shown that single-layer graphene can stimulate proliferation of human osteoblast-like cell line (SAOS-2). They suggested that graphene produced by chemical vapor deposition and transferred to other surfaces (in our case glass slide) causes many ripples and wrinkles in graphene layer and this can affect proliferation and also cell adhesion. They also have concluded that hydrophobic surface of graphene treated with hydrogen enhances proliferation of SAOS-2 cells better than hydrophilic surface of graphene treated with oxygen (Kalbacova et al., 2014). Liu et al. (2016) have examined HepG2, A549, MCF-7, and HeLa cells treated with graphene and noticed enhanced cell proliferation in all tested cell cultures even up to 60%. They have suggested that it was due to the activation of the epidermal growth factor receptor.

Fibroblasts are pivotal to tissue repair and tissue remodeling; they migrate into the wound site and proliferate. Various peptide growth factors stimulate fibroblasts to migrate into the wound area. On the contrary, chronic wound fibroblasts are unresponsive to growth factors (Kim et al., 2003). Cell migration is a self-mechanical phenomenon involving internal molecular actuators. During this process, contraction

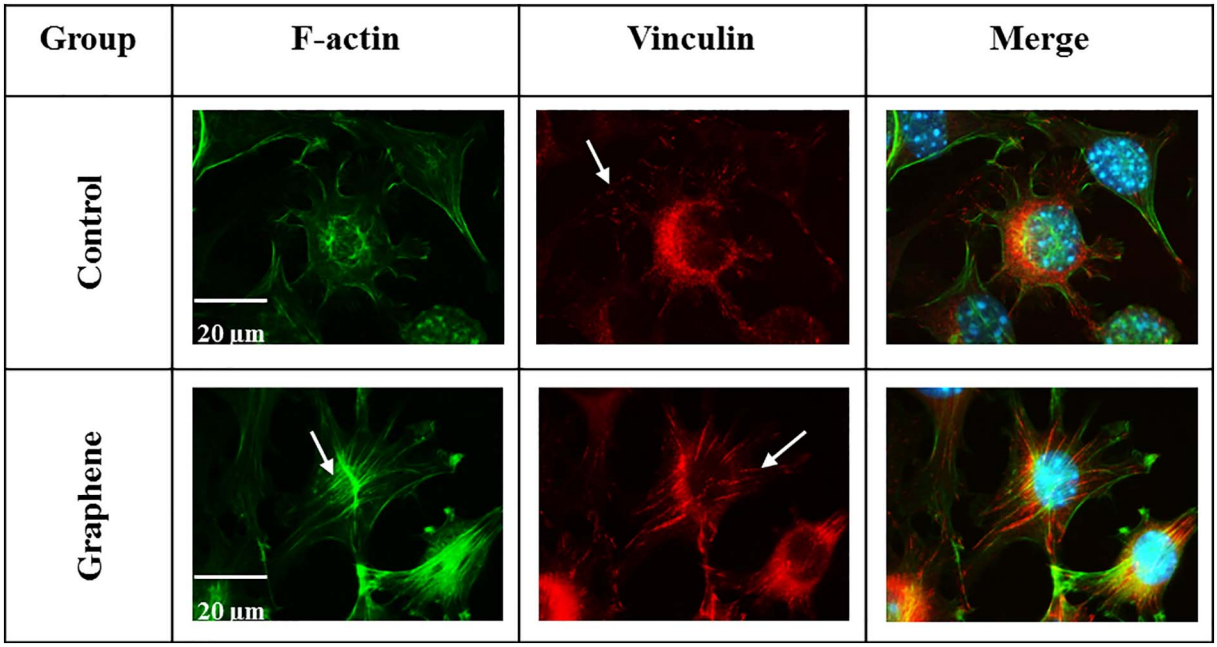

Fig. 9. The architecture of actin cytoskeleton and focal adhesion structures in L929 cells. Cells were incubated for 24 h on glass and pristine graphene monolayer and stained with phalloidin-FITC (F-actin, green fluorescence), anti-vinculin Abs (vinculin, red fluorescence) and Hoechst 33,342 (DNA, blue fluorescence). Arrows indicate actin stress fibers (left panel) and focal adhesion protein – vinculin (middle panels). (For interpretation of the references to color in this figure legend, the reader is referred to the web version of this article.)

forces are generated, focal complexes that connect the cell with the external environment are created, polymerization and depolymerization of the actin filaments that form the lamellipodia and filopodia occur, and all these processes facilitate internal reconstruction (Tojkander et al., 2012; Lange and Fabry, 2013). This spatial organization of cytoskeletal components is regulated by mutually linked signaling pathways and feedback mechanisms that influence the kinetics of physiological changes leading to cell polarization and migration (Welf and Haugh, 2011). The cell adhesion to the substrate on which cell moves is prerequisite for an active cell migration. Migration of fibroblast can be observed *in vitro* in the "wound space" of an artificially ruptured monolayer. To repair tissue damage, cells on the wound edge must move in a coordinated way (Trepat et al., 2012). Migration of L929 cells on graphene substrate was organized and proceeded in an orderly manner, whereas in the control group (glass substrate) at 12 h of incubation migration was less organized and cells from both wound edges gradually filled the central part of the wound. We suppose that different spreading and migration behavior of L929 cells is a consequence of cells attached to different substrates: glass and graphene. Generally, with higher stiffness, cells spread more and contract stronger, but migrate more slowly (Lange and Fabry, 2013). Although glass and plastic are rigid surfaces where most animal cell types grow *in vitro*, the graphene surface induces greater mechanical stress in the cells, which alter conformation of mechanosensitive focal adhesion proteins, for example vinculin. Focal adhesions are the focal complex structure that ensures proper communication between the cell and the extracellular matrix and response to environmental stress (Tojkander et al., 2012; Furuhashi et al., 2012). Vinculin modulates the dynamics of cell adhesion and movement. The decrease in vinculin expression results in increased cell migration (Furuhashi et al., 2012; Wytrwal et al., 2016). The properties of the substrate on which the cells migrate affect cell morphology, for example, the cells cultured on a rigid substrate have marked prominent stress fibers and focal adhesions and they are aligned along the major cell axis (Tojkander et al., 2012; Wytrwal et al., 2016). Kalbacova et al. (2010) have showed *in vitro* that SAOS-2 and mesenchymal stromal cells (MSC) better adhered to graphene substrate than to SiO_2. SAOS-2 and MSC adhesion was characterized by immunofluorescence staining of vinculin and actin filaments. Tan et al. (2015) have showed comparable adhesion (based on vinculin and paxillin staining) of human corneal stromal fibroblasts to graphene and titanium substrates. The average number of focal contacts per cell in SAOS-2 incubated for 2 h in the presence of FBS on graphene treated with hydrogen and on the polystyrene was 25 and 30, respectively (Kalbacova et al., 2014). Vogler et al. (2013) have estimated the number of focal adhesions in the L929 fibroblasts based on immunofluorescent staining of vinculin for about 40 per cell. Cells maintained under hypoxia condition were characterized by significantly higher number of focal adhesions (Vogler et al., 2013), similarly in our cells grown on graphene (approximately 60 per cell). Hypoxia occurs during wound healing, when blood vessels are injured or damaged. Our results indicate that stress induced by graphene substrates results in the formation of more focal adhesions, as in the hypoxia state.

Kalbacova et al. (2014) have recommended evaluating the adhesion 2 h after cell seeding. In our experiments we assessed the number of focal adhesion after 24 h, because we wanted to check the behavior of migrating cells into the wound. The graphene substrate causes a more linear cell migration than uncoated glass but the wound closure occurs within 48 h in both cultures *i.e.*, graphene and the glass substrate. Furuhashi et al. (2012) have suggested that fibroblasts not only adhere to the substrate, but also adapt to the topography of its surface. We suspected that environmental stress caused by the presence of graphene (its topography) could change size of L929 cells. Vogler et al. (2013) have stated that hypoxia causes enlargement of L929 cell area (almost 2-fold), increases spread of cells but slows down migration. In our study the area of cells migrating on the graphene leading to closure of the wound was only slightly higher ($p > 0.05$) compared to the glass substrate (control group). Min-max values were within average range in control and graphene group: 260–2700 and 270–5500 μm^2, and median oscillated around 1000 and 1072 μm^2, respectively. Verdanova et al. (2017) have presented that the average cell area of primary human fibroblasts cultivated on tissue culture polystyrene for 2 h, with or without FBS, was 1434 and 2107 μm^2, respectively. The average surface area of our cells line L929 was 1068 ± 455 μm^2 for control group and 1128 ± 497 μm^2 for graphene substrate. The average cell area of human osteoblasts (SASO-2) grown on graphene samples after 48 h of incubation, with 15% addition of FBS, was between 1100 and 1300 μm^2

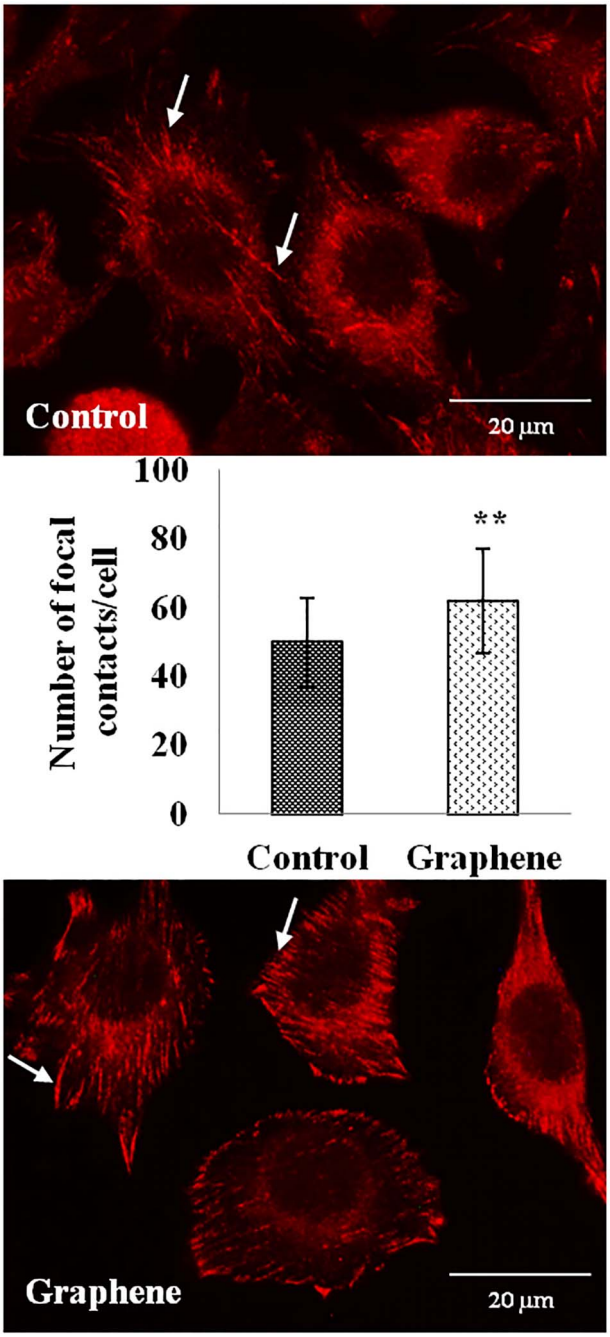

Fig. 10. Focal contacts in L929 fibroblasts grown on glass and graphene. Arrows indicate focal contacts. Focal contacts per cell were counted after 24 h of incubation. Data are presented as mean ± SD (standard deviation) of three independent experiments. $^{**}p < 0.01$.

and smaller to those obtained on polystyrene substrate, but cells seeded on graphene spread faster. Taken together, L929 cells cultured on graphene produced more focal adhesions probably in reactions to graphene topography, however the cell area was not affected. Cells were normal, not enlarged, and cytoskeletal integrity was maintained. Moreover, cell polymerization and contractility during migration occurred, what indicated the proper functioning of the cells.

5. Conclusion

Graphene is non-toxic to L929 cells, causes linear migration of cells to close the wound, increases number of focal adhesions (based on vinculin staining) and cell proliferation (using WST-8). The above findings suggest that graphene could be beneficial for tissue damage recovery.

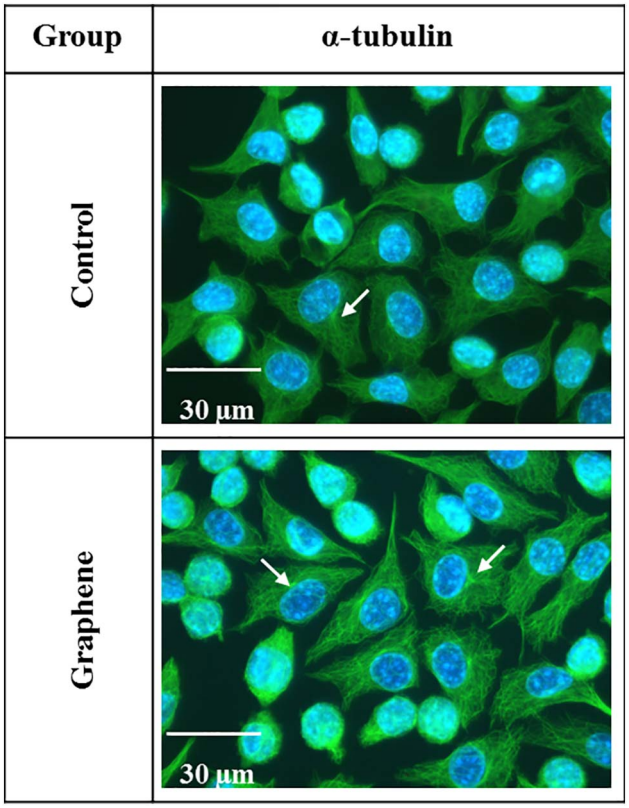

Fig. 11. Immunofluorescence detection of α-tubulin. L929 cells grown on glass or graphene coverslips for 24 h were fixed in cold methanol. The fixed cells were stained for α-tubulin (green fluorescence) and DNA (blue fluorescence). Arrows indicate microtubule-organizing center (MTOC) in the perinuclear region of cells. (For interpretation of the references to color in this figure legend, the reader is referred to the web version of this article.)

Conflict of interest

The authors declare that there are no conflicts of interest.

Transparency document

The http://dx.doi.org/10.1016/j.tiv.2018.01.028 associated with this article can be found, in online version.

Acknowledgement

We are grateful to Tomasz Jurkowicz for inspiration and assistance of this work. We thank Dr. Felix N. Toka for his valuable help with manuscript editing.

Funding

This work was supported by the Warsaw University of Life Sciences [grants number 505-10-072500-M00320-99 and 505-10-072500-N00266-99].

References

Akhan, O., Ghaderi, E., 2010. Toxicity of graphene and graphene oxide nanowalls against bacteria. ACS Nano 4 (10), 5731–5736.
Atherton, P., Stutchbury, B., Wang, D.-Y., Jethwa, D., Tsang, R., Meiler-Rodriguez, E.,

Wang, P., Bate, N., Zent, R., Barsukov, I.L., Goult, B.T., Critchley, D.R., Ballestrem, C., 2015. Vinculin controls talin engagement with the actomyosin machinery. Nat. Commun. 6, 1–12.
Bacakova, L., Filova, E., Parizek, M., Ruml, T., Svorcik, V., 2011. Modulation of cell adhesion, proliferation and differentiation on materials designed for body implants. Biotechnol. Adv. 29, 739–767.
Burridge, K., Mangeat, P., 1984. An interaction between vinculin and talin. Nature 308 (5961), 744–746.
Chen, G.-Y., Pang, D.W.-P., Hwang, S.-M., Yuan, H.-Y., Hu, Y.-C., 2012. A graphene-based platform for induced pluripotent stem cells culture and differentiation. Biomaterials 33, 418–427.
Ciuk, T., Pasternak, I., Krajewska, A., Sobieski, J., Caban, P., Szmidt, J., Strupinski, W., 2013. Properties of chemical vapor deposition graphene transfer red by high-speed electrochemical delamination. J. Phys. Chem. C 117 (40), 20833–20837.
DeMali, K.A., Sun, X., Bui, G.A., 2014. Force transmission at cell–cell and cell–matrix adhesions. Biochemistry 53 (49), 7706–7717.
Ferrari, A.C., Meyer, J.C., Scardaci, V., Casiraghi, C., Lazzeri, M., Mauri, F., Piscanec, S., Jiang, D., Novoselov, K.S., Roth, S., et al., 2006. Raman Spectrum of graphene and graphene layers. Phys. Rev. Lett. 97, 189401.
Furuhashi, A., Ayukawa, Y., Atsuta, I., Okawachi, H., Koyano, K., 2012. The difference of fibroblast behavior on titanium substrata with different surface characteristics. Odontology 100, 199–205.
Goenka, S., Sant, V., Sant, S., 2014. Graphene-based nanomaterials for drug delivery and tissue engineering. J. Control. Release 173, 75–88.
Graf, D., Molitor, F., Ensslin, K., Stampfer, C., Jungen, A., Hierold, C., Wirtz, L., 2007. Spatially resolved Raman spectroscopy of single- and few-layer graphene. Nano Lett. 7, 238–242.
Guo, X., Mei, N., 2014. Assessment of toxic potential of graphene family nanomaterials. J. Food Drug Anal. 22 (1), 105–115.
Gupta, A., Chen, G., Joshi, P., Tadigadapa, S., Eklund, P.C., 2006. Raman scattering from high-frequency phonons in supported n graphene layer films. Nano Lett. 6, 2667–2673.
Gurunathan, S., Han, J.W., Kim, E., Kwon, D.-N., Park, J.-K., Kim, J.-H., 2014. Enhanced green fluorescent protein- mediatel synthesis of biocompatible graphene. J. Nanobiotechnol. 12 (41), 1–16.
ISO: No. 10993-5, 2009. Biological Evaluation of Medical Devices - Tests for in vitro Cytotoxicity.
Jesion, I., Skibniewski, M., Skibniewska, E., Strupiński, W., Szulc-Dąbrowska, L., Krajewska, A., Pasternak, I., Kowalczyk, P., Pińkowski, R., 2015. Graphene and carbon nanocompounds: biofunctionalization and applications in tissue engineering. Biotechnol. Biotechnol. Equip. 29, 415–422.
Kalbacova, M., Broz, A., Kong, J., Kalbac, M., 2010. Graphene substrates promote adherence of human osteoblasts and mesenchymal stromal cells. Carbon 48, 4323–4329.
Kalbacova, M., Verdanova, M., Broz, A., Vetushka, A., Fejfar, A., Kalbac, M., 2014. Modulated surface of single-layer graphene controls cell behavior. Carbon 72, 207–214.
Kim, B.C., Kim, H.T., Park, S.H., Cha, J.S., Yufit, T., Kim, S.J., Falanga, V., 2003. Fibroblasts from chronic wounds show altered TGF-beta-signaling and decreased TGF-beta type II receptor expression. J. Cell. Physiol. 195 (3), 331–336.
Lange, J.R., Fabry, B., 2013. Cell and tissue mechanics in cell migration. Exp. Cell Res. 319, 2418–2423.
Lee, D.S., Riedl, C., Krauss, B., von Klitzing, K., Starke, U., Smet, J.H., 2008. Raman spectra of epitaxial graphene on SiC and of epitaxial graphene transferred to SiO2. Nano Lett. 9, 4320–4325.
Lee, S.K., Kim, H., Shim, B.S., 2013. Graphene: an emerging material for biological tissue engineering. Carbon Lett. 14 (2), 63–75.
Liao, K.-H., Lin, Y.S., Macosko, C.W., Haynes, C.L., 2011. Cytotoxicity of graphene oxide and graphene in human erythrocytes and skin fibroblasts. ACS Appl. Mater. Interfaces 3 (7), 2607–2615.
Liu, W., Sun, C., Liao, C., Cui, L., Li, H., Qu, G., Yu, W., Song, N., Cui, Y., Wang, Z., Xie, W., Chen, H., Zhou, Q., 2016. Graphene enhances cellular proliferation through activating the epidermal growth factor receptor. J. Agric. Food Chem. 64 (29), 5909–5918.
Mogilner, A., Keren, K., 2009. The shape of motile cells. Curr. Biol. 19 (17), 762–771.
Park, J.C., Park, B.J., Lee, D.H., Suh, H., Kim, D.G., Kwon, O.H., 2002. Evaluation of the cytotoxicity of polyetherurethane (PU) film containing zinc diethyldithiocarbamate (ZDEC) on various cell lines. Yonsei Med. J. 43 (4), 518–526.
Park, S., An, J., Jung, I., An, S.J., Li, X., Velamakanni, A., Ruoff, R.S., 2009. Colloidal suspensions of highly reduced graphene oxide in a wide variety of organic solvents. Nano Lett. 9 (4), 1593–1597.
Peng, X., Nelson, E.S., Maiers, J.L., DeMali, K.A., 2011. New insights into vinculin function and regulation. Int. Rev. Cell Mol. Biol. 287, 191–231.
Poskus, L.T., Lima, R.S.M.S., Lima, I.R., Guimarães, J.G.A., da Silva, E.M., Granjeiro, J.M.G., 2009. Cytotoxicity of current adhesive systems: in vitro testing on cell culture of L929 and balb/c 3T3 fibroblasts. Rev. Odonto Ciênc. 24 (2), 129–134.
Saunders, R.M., Holt, M.R., Jennings, L., Sutton, D.H., Barsukov, I.L., Bobkov, A., Liddington, R.C., Adamson, E.A., Graham, A.D., Crichley, D.R., 2006. Role of vinculin in regulating focal adhesion turnover. Eur. J. Cell Biol. 85 (6), 487–500.
Sawosz, E., Jaworski, S., Kutwin, M., Vadalasetty, K.P., Grodzik, M., Wierzbicki, M., Kurantowicz, N., Strojny, B., Hotowy, A., Lipińska, L., Jagiełło, J., Chwalibog, A., 2015. Graphene functionalized with arginine decreases the development of glioblastoma Multiforme tumor in gene-dependent manner. Int. J. Mol. Sci. 16, 25214–25233.
Schliwa, M., Blerkom, J., 1981. Structural interaction of cytoskeletal components. J. Cell Biol. 90, 222–235.
Stehbens, S., Wittmann, T., 2012. Targeting and transport: how microtubules control focal adhesion dynamics. J. Cell Biol. 198, 481–489.
Strupinski, W., inventor; Instytut Technologii Materialow Elektronicznych, assignee. Method of graphene manufacturing. European patent EP 2392547 A2. 2011 (Dec 7).
Strupinski, W., Grodecki, K., Wysmolek, A., Stepniewski, R., Szopek, T., Gaskell, P.E., Grüneis, A., Haberer, D., Bozek, R., Krupka, J., Baranowski, J.M., 2011. Graphene epitaxy by chemical vapor deposition on SiC. Nano Lett. 11 (4), 1786–1791.
Szulc-Dabrowska, L., Gregorczyk, K.P., Struzik, J., Boratynska-Jasinska, A., Szczepanowska, J., Wyzewski, Z., Toka, F.N., Gierynska, M., Ostrowska, A., Niemiałtowski, M.G., 2016. Remodeling of the fibroblast cytoskeletal architecture during the replication cycle of Ectromelia virus: a morphological in vitro study in a murine cell line. Cytoskeleton 73, 396–417.
Tan, X.W., Thompson, B., Konstantopoulos, A., Goh, T.W., Setiawan, M., Yam, G.H., Tan, D., Khor, K.A., Mehta, J.S., 2015. Application of graphene as candidate biomaterial for synthetic Keratoprosthesis skirt. Invest. Ophthalmol. Vis. Sci. 56 (11), 6605–6611.
Tojkander, S., Gateva, G., Lappalainen, P., 2012. Actin stress fibers- assembly, dynamics and biological roles. J. Cell Sci. 125, 1855–1864.
Trepat, X., Chen, Z., Jacobson, K., 2012. Cell migration. Compr. Physiol. 2 (4), 2369–2392.
Tschumperlin, D.J., 2013. Fibroblasts and the ground they walk on. Physiology 28, 380–390.
Verdanova, M., Rezek, B., Broz, A., Ukraintsev, E., Babchenko, O., Artemenko, A., Izak, T., Kromka, A., Kalbac, M., Hubalek, Kalbacova M., 2016. Nanocarbon allotropes - graphene and Nanocrystalline diamond - promote cell proliferation. Small 12, 2499–2509.
Verdanova, M., Sauerova, P., Hempel, U., Kalbacova, M., 2017. Initial cell adhesion of three cell types in the presence and absence of serum proteins. Histochem. Cell Biol. http://dx.doi.org/10.1007//s00418-017-1571-7.
Vogler, M., Vogel, S., Krull, S., Farhat, K., Leisering, P., Lutz, S., Wuertz, C.M., Katschinski, D.M., Zieseniss, A., 2013. Hypoxia modulates Fibroblastics architecture, adhesion and migration: a role for HIF-1α in Cofilin regulation and cytoplasmic actin distribution. PLoS One 8 (7), e69128.
Wang, Y., Li, Z., Wang, J., Li, J., Lin, Y., 2011. Graphene and graphene oxide: biofunctionalization and applications in biotechnology. Trends Biotechnol. 29 (5), 205–212.
Wang, B., Luo, P.G., Teckett II, K.N., Ruiz, O.N., Bunker, C.E., Cheng, S.H., Parenzan, A., Sun, Y.-P., 2012. Graphene oxide as substrate for enhanced mammalian cell growth. J. Nanomater. Mol. Nanotechnol. 1, 2.
Wang, W., Caetano, G., Ambler, W.S., Blaker, J.J., Frade, M.A., Mandal, P., Diver, C., Bartolo, P., 2016. Enhancing the hydrophilicity and cell attachment of 3D printed PCL/graphene scaffolds for bone tissue engineering. Materials 9 (992), 1–11.
Welf, E.S., Haugh, J.M., 2011. Signaling pathways that control cell migration: models and analysis. Wiley Interdiscip. Rev. Syst. Biol. Med. 3 (2), 231–240.
Wojtoniszak, M., Chen, X., Kalenczuk, R.J., Wajda, A., Łapczuk, J., Kurzewski, M., Drozdzik, M., Chu, P.K., Borowiak-Palen, E., 2012. Synthesis, dispersion, and cytocompatibility of graphene oxide and reduced graphene oxide. Colloids Surf. B: Biointerfaces 89, 79–85.
Wytrwal, M., Koczurkiewicz, P., Zrubek, K., Niemiec, W., Michalik, M., Kozik, B., Szneler, E., Bernasik, A., Madeja, Z., Nowakowska, M., Kepczynski, M., 2016. Growth and motility of human skin fibroblasts on multiplayer strong polyelectrolyte films. J. Colloid Interface Sci. 461, 305–316.
Yao, M., Goult, B.T., Chen, H., Cong, P., Sheetz, M.P., Yan, J., 2014. Mechanical activation of vinculin binding to talin locks talin in an unfolded conformation. Sci. Rep. 4 (4610), 1–7.
Zhang, B., Wei, P., Zhou, Z., Wei, T., 2016. Interactions of graphene with mammalian cells: molecular mechanisms and biomedical insights. Adv. Drug Deliv. Rev. 105, 145–162.
Zhou, L., Forman, H.J., Ge, Y., Lunec, J., 2017. Multi-walled carbon nanotubes: a cytotoxicity study in relation to functionalization, dose and dispersion. Toxicol. in Vitro 42, 292–298.